Subscriber access provided by UNIV TWENTE

Article

Localized Triggering of the Insulator-Metal Transition in VO Using a Single Carbon Nanotube

Stephanie M. Bohaichuk, Miguel Muñoz Rojo, Gregory Pitner, Connor J. McClellan, Feifei Lian, Jason Li, Jaewoo Jeong, Mahesh G. Samant, Stuart S. P. Parkin, H.-S. Philip Wong, and Eric Pop

ACS Nano, **Just Accepted Manuscript** • DOI: 10.1021/acsnano.9b03397 • Publication Date (Web): 08 Aug 2019

Downloaded from pubs.acs.org on August 19, 2019

Just Accepted

"Just Accepted" manuscripts have been peer-reviewed and accepted for publication. They are posted online prior to technical editing, formatting for publication and author proofing. The American Chemical Society provides "Just Accepted" as a service to the research community to expedite the dissemination of scientific material as soon as possible after acceptance. "Just Accepted" manuscripts appear in full in PDF format accompanied by an HTML abstract. "Just Accepted" manuscripts have been fully peer reviewed, but should not be considered the official version of record. They are citable by the Digital Object Identifier (DOI®). "Just Accepted" is an optional service offered to authors. Therefore, the "Just Accepted" Web site may not include all articles that will be published in the journal. After a manuscript is technically edited and formatted, it will be removed from the "Just Accepted" Web site and published as an ASAP article. Note that technical editing may introduce minor changes to the manuscript text and/or graphics which could affect content, and all legal disclaimers and ethical guidelines that apply to the journal pertain. ACS cannot be held responsible for errors or consequences arising from the use of information contained in these "Just Accepted" manuscripts.

is published by the American Chemical Society. 1155 Sixteenth Street N.W., Washington, DC 20036

Published by American Chemical Society. Copyright © American Chemical Society. However, no copyright claim is made to original U.S. Government works, or works produced by employees of any Commonwealth realm Crown government in the course of their duties.

Localized Triggering of the Insulator-Metal Transition in VO_2 Using a Single Carbon Nanotube

Stephanie M. Bohaichuk,[1] Miguel Muñoz Rojo,[1,2] Gregory Pitner,[1] Connor J. McClellan,[1] Feifei Lian,[1] Jason Li,[3] Jaewoo Jeong,[4] Mahesh G. Samant,[4] Stuart S. P. Parkin,[4] H.-S. Philip Wong,[1] Eric Pop[1,5,*]

[1]Dept. of Electrical Engineering, Stanford University, Stanford, CA 94305, USA
[2]Dept. of Thermal and Fluid Engineering, University of Twente, 7500 AE Enschede, Netherlands
[3]Asylum Research, Santa Barbara, CA 93117, USA
[4]IBM Almaden Research Center, San Jose, CA 95120, USA
[5]Dept. of Materials Science and Engineering, Stanford University, Stanford, CA 94305, USA

ABSTRACT: Vanadium dioxide (VO_2) has been widely studied for its rich physics and potential applications, undergoing a prominent insulator-metal transition (IMT) near room temperature. The transition mechanism remains highly debated, and little is known about the IMT at nanoscale dimensions. To shed light on this problem, here we use ~1 nm wide carbon nanotube (CNT) heaters to trigger the IMT in VO_2. Single metallic CNTs switch the adjacent VO_2 at less than half the voltage and power required by control devices without a CNT, with switching power as low as ~85 μW at 300 nm device lengths. We also obtain potential and temperature maps of devices during operation using Kelvin Probe Microscopy (KPM) and Scanning Thermal Microscopy (SThM). Comparing these with three-dimensional electrothermal simulations, we find that the local heating of the VO_2 by the CNT plays a key role in the IMT. These results demonstrate the ability to trigger IMT in VO_2 using nanoscale heaters, and highlight the significance of thermal engineering to improve device behaviour.

KEYWORDS: vanadium dioxide, insulator-metal transition, carbon nanotube, scanning probe microscopy

*Contact: epop@stanford.edu

Materials with an abrupt insulator-metal transition (IMT) have garnered much interest, both as a study of the role of electron correlations in creating new electronic phases, and for their variety of potential applications in optics and electronics.[1,2] Vanadium dioxide (VO_2) has one of the most pronounced transitions among these, with a structural transition from monoclinic to rutile at ~340 K. This results in a drop in resistivity by up to five orders of magnitude, accompanied by significant changes in optical properties.[3,4] This transition can be induced electrically on a sub-nanosecond time scale by using current flow, and reverses once the stimulus is removed.[5] These properties have made VO_2 a candidate for threshold switches and selectors,[6-8] transistors,[9,10] oscillators,[11,12] and tunable metamaterials for optoelectronics.[13-16]

Integrating IMT materials with current semiconductor technology to build these applications will require knowledge of their behaviour at nanoscale dimensions. For example, electrical devices based on two-terminal switching of VO_2 are expected to offer faster,[5] lower voltage,[17-19] and lower energy[2] switching as they are reduced to smaller dimensions, similar to devices based on phase-change materials like $Ge_2Sb_2Te_5$.[20,21] Most two-terminal VO_2 devices studied to date have had dimensions ranging from ~20 nm to a few microns,[19] with IMT behaviour preserved in all cases. It remains to be seen if the IMT in electrical devices changes once even smaller dimensions are reached. Moreover, the nanoscale triggering mechanism of VO_2 is not completely understood, with some debate on the role of Joule heating[22] vs. electric field effects and carrier injection.[23,24] The distinction partly arises from the origin of the IMT (*e.g.* a Peierls structural transition triggered by heating and electron-phonon coupling *vs.* a Mott electronic transition based on carrier concentration), and will provide insight into the types of devices that can be designed.

In this work, we probe the mechanism of VO_2 switching at the nanoscale. To extend below the limits of lithography we use single-wall metallic carbon nanotube (CNT) heaters to trigger the VO_2 transition. Due to their ~1 nm diameter, such metallic CNTs are ideal candidates for probing a nanoscale phase change or IMT, as Joule heaters (capable of reaching ~600ºC in air, and ~2000ºC in vacuum) or electrodes.[25,26] By using the localized heating of a metallic CNT we are able to initiate the IMT at the nanoscale, at a lower power than relying on Joule heating in the VO_2 itself, which is promising for the development of applications requiring nanoscale VO_2 devices. We also use Kelvin Probe Microscopy (KPM) and Scanning Thermal Microscopy (SThM) to obtain high resolution spatial maps of the electric potential and temperature changes in our devices during operation, to understand their switching mechanism. We find good agreement between our experimental results and electrothermal simulations, confirming that Joule heating plays a major role in our devices, both with and without a CNT.

RESULTS AND DISCUSSION

We fabricated nearly one thousand two-terminal VO_2 devices with and without CNTs on top. Aligned CNT arrays were grown on a separate quartz substrate, then transferred[27] onto thin films of single crystal VO_2 grown epitaxially[28] on TiO_2 (101), as illustrated in Figure 1a–d. The CNTs were coated with 100 nm of Au by electron-beam (e-beam) evaporation, then peeled off the quartz and transferred onto VO_2 using thermal release tape. The Au was wet-etched to leave only CNTs on VO_2 (see Methods for additional details). A scanning electron microscope (SEM) image of transferred CNTs on VO_2 is shown in Figure 1e. Excess CNTs were removed and the VO_2 was wet etched into stripes (Figure 1f, also see Methods). E-beam evaporated Pd contacts were added to make complete devices, as shown in Figure 1g,h.

We used electrical testing and atomic force microscopy (AFM) scans to select devices with single metallic CNTs for further study, and for comparison to control devices without a CNT. (The selection process, and comparisons with multiple-CNT or with semiconducting-CNT devices are described in the Supporting Information Section 2.) Figure 1g shows the schematic of a VO_2 device with a single CNT heater, both extending underneath Pd contacts. A series resistor R_S is used as a current compliance to protect devices from overheating failure in the metallic state, and to reduce current overshoot from external capacitance (*e.g.* cables and probe arm). The R_S value (20 – 200 kΩ) is chosen to be a small fraction of the insulating VO_2 resistance, but higher than the metallic VO_2 resistance, as detailed in the Supporting Information Section 2. Figure 1h shows an optical image of a shorter device, fabricated by adding Pd contact extensions. The measured resistance of a VO_2 device without a CNT is shown in Figure 1i as a function of stage temperature, displaying the transitions at 328 K and 321 K for heating (T_{IMT}) and cooling (T_{MIT}) respectively, and a change in resistance over three orders of magnitude.

Figure 2a compares typical measured voltage-controlled I-V characteristics of VO_2 devices with and without a CNT (L = 6 μm) at room temperature (T_0 = 296 K). Electrical switching is repeatable and independent of bias polarity, with similar behaviour consistently observed across hundreds of devices. The non-CNT device behaves linearly as a resistor, until significant Joule heating begins to occur. As the VO_2 temperature increases, it becomes more conductive and the I-V curve is increasingly superlinear. Once the transition occurs at a critical voltage V_{IMT}, most of the applied bias is dropped across R_S, causing a snapback in device voltage. In the metallic state R_S dominates over the VO_2 resistance, limiting the maximum current, power, and on/off ratio observed. Because R_S is used to limit heating, if devices were operated at much shorter time scales, then R_S could likely be reduced, recovering more of the intrinsic on/off ratio of the VO_2.

R_S can also be used to control the resistance and volume of the VO_2 that is metallic (Supporting Information Figure S8).

There are significant differences in the *I-V* characteristics when a single metallic CNT is present. Prior to the IMT there is higher current and a sublinear behaviour typical of current saturation due to self-heating in the CNT.[29] The IMT of the VO_2 occurs at much lower power, because the (hot) CNT is able to switch a highly localized VO_2 region at significantly lower voltage compared to Joule heating through the entire VO_2. Once an initial region of VO_2 below the CNT has switched, the increased current from the metallic VO_2 becomes self-sustaining and the metallic region can expand, leading to a large and abrupt increase in current. The metal-insulator transition (MIT) that occurs when the voltage is ramped back down is unaffected by the CNT, which no longer carries the majority of the current once the voltage snapback occurs. Hysteresis is observed in both types of devices because $T_{IMT} \neq T_{MIT}$ and because at a given voltage, metallic VO_2 will cause more heating ($\propto V^2/R$) than insulating VO_2. Due to the reduction in V_{IMT}, devices with a CNT have a significantly smaller total hysteresis window. As expected, both types of devices show a decrease in V_{IMT} with rising ambient temperature (Supporting Information Section 2). At all temperatures measured, devices with a CNT display lower switching voltage and power compared to control devices without a CNT.

These differences in *I-V* characteristics of VO_2 devices with and without a CNT are also seen at shorter length scales (*i.e*. Pd contact separation), shown in Figure 2b. Switching is consistently triggered by the ~1 nm wide CNT at all length scales, shown in Figured 2c–d. The presence of a CNT halves the required switching voltage and power in all devices measured, including our shortest 300 nm lengths. Figure 2c shows that switching voltage scales linearly with length for both devices types. (Width scaling of our VO_2 devices is displayed in Supporting Information Figures S4 and S15.) Shorter devices have lower resistance and higher Joule heating at a given voltage, thus requiring a lower voltage and power for switching. An effective switching field can be extracted from the slope of the linear fits in Figure 2c, giving 3.5 ± 0.2 V/μm with a CNT and 7.6 ± 0.2 V/μm without, though this does not necessarily indicate a field-switching mechanism. If switching were triggered by field effects such as carrier injection, then the field extracted would be a description of the VO_2 quality and the efficiency of the switching mechanism. For a Joule heating mechanism, the field would be determined by the electrical and thermal properties of the materials that set the maximum device temperature (including ambient temperature, uniformity of heating, thermal conductivities and thermal boundary resistances, resistivities, *etc*.).

The vertical axis intercept in Figure 2c (2.0 ± 0.8 V with a CNT, and 6.8 ± 1.0 V without) characterizes the voltage drop (contact resistance) and heat loss at the contacts.[19] This intercept depends on the contact material[17] and its temperature-dependent contact resistivity.[30,31] The large difference between the intercept of devices with and without a CNT is likely due to a lower contact resistance to the CNT than the VO_2. An estimate of the contact resistance at switching can be found using the intercept and typical switching currents (Supporting Information Figure S3), giving 32 ± 15 kΩ and 123 ± 48 kΩ for devices with and without a CNT, respectively. This is consistent with other estimates (Supporting Information Section 2),[29, 32] but due to non-uniform current flow a full interpretation of these values is difficult. The ratio between the voltage drop at the contacts and the effective switching field yields a characteristic length below which the switching voltage could be contact-dominated, ~0.6 μm and ~0.9 μm in our devices with and without a CNT respectively. Although the power reduction observed in devices with a CNT comes partly from localized switching reducing the required field, a significant part comes from the difference in contacts, which could limit the switching voltage and temperature in nanoscale thin film devices.

Given that the switching current is similar between devices with and without CNTs for the device dimensions used (Supporting Information Figure S3), Figure 2d shows that there is a reduction in power at all length scales by using a CNT. Normalization by VO_2 width is appropriate for devices without a CNT, but adds spread in the P_{IMT} of devices with a CNT, whose switching does not depend on the VO_2 width. Power scales linearly with device length, and our shortest devices with and without a CNT have switching powers of 85 μW and 260 μW respectively, among the lowest reported at similar $\Delta T = T_{\mathrm{IMT}} - T_0$.[6, 19] It is expected that further reducing our device length and width would reduce switching power. These results demonstrate the feasibility of VO_2 switching down to the nanoscale, with its IMT behaviour preserved, and that there are power benefits to doing so.

The debate regarding thermal and non-thermal IMT effects prompts us to examine whether our electrical results can be explained solely by Joule heating. To gain insight into the switching mechanism of devices with a CNT, we utilize KPM and SThM scanning probe techniques. KPM is a non-contact scanning probe technique that detects changes in the surface potential across a sample.[33] We use KPM to study the potential in biased VO_2 devices with and without a CNT. On the other hand, SThM is a contact-mode scanning probe technique that uses a thermo-resistive probe sensitive to temperature changes on the surface of a sample with a spatial resolution of <100 nm.[34,35] We use SThM to study the heating profile of biased devices in order to identify the thermal contribution of the CNT to the IMT of the VO_2.

Figure 3a shows a topographic scan of a VO_2 device without a CNT, and Figures 3b–d show KPM results for that device, with applied voltages V_S as labelled. Scans are centered on the VO_2 channel with the TiO_2 substrate revealed along the left and right edges. The small spots are carbon-based residue from processing. The contacts are just outside the scan with the grounded electrode at the top and the positive electrode at the bottom, connected to R_S = 200 kΩ. Figure 3b shows a KPM scan with no bias across the device. The VO_2 appears uniform, with a slight contrast against the process residues and TiO_2. Figures 3c and 3d show KPM scans taken with a constant voltage V_S applied, (c) in the insulating state and (d) once the VO_2 has electrically switched to the metallic state. In biased devices, there is a linear decrease in potential from the positive electrode to the grounded electrode (see Supporting Information Section 3). The scans have been processed with a first order line flattening operation to remove this, highlighting local differences in surface potential across the device width. In both states, the device has for the most part a nearly uniform potential drop across it with no strongly localized fields. In the metallic state some slight variation exists across the width of the device from local differences in temperature and conductivity.

Figure 3e shows a topographic scan of a VO_2 device with a CNT, and Figures 3f–h show KPM results for the device, with potential variation across the width that differs significantly from the non-CNT device. The orientation of the electrodes relative to the images is the same, with the VO_2 edges just outside the scan on the left/right. These images were processed in the same way. Although the raw potential drop is linear, flattening reveals a small local concentration of the surface potential around the CNT in the insulating state (g). Once the device switches to the metallic state (h) and voltage snapback occurs, the flattened potential appears much more uniform across the device, with the CNT having little effect anymore.

The contrast in the potential across the devices with and without a CNT indicates that the CNT has a large impact on the VO_2 switching. This could be a result of field enhancement, or due to a thermally-induced change in VO_2 conductivity or workfunction. To test whether this can be attributed to thermal effects, we perform SThM on a similar VO_2 device with a CNT. Figures 4a and 4b show topographic scans of this device before and after capping with a 50 nm layer of poly(methyl methacrylate) (PMMA), with the CNT no longer visible after capping. This PMMA layer is needed for electrical insulation between the SThM probe and sample surface. The contacts are at the top and bottom of the image, and the device is held at a constant voltage, V_S = 17 V, with R_S = 200 kΩ. The SThM results in Figure 4c prior to switching confirm that there is significant localized heating around the CNT.

To quantify the local temperature rise in the VO_2 induced by the CNT, we perform three-dimensional (3D) finite element simulations which self-consistently consider electrical, thermal, and Joule heating effects. The electrical conductivity of both the CNT and the VO_2 are described as a function of temperature (Supporting Information Section 4). We also include electrical contact resistances and thermal boundary resistances, which cannot be neglected. The simulated device has the same dimensions as the real device scanned by SThM, capped by 50 nm of PMMA with a CNT at the device center. Simulating the device at the same bias as the SThM scan, we see in Figure 4d a similar temperature profile on the PMMA surface compared to the real device. Figure 4e shows that we can reproduce the experimental *I-V* curve, with the simulated device having $V_{\mathrm{IMT}} \sim 20$ V. Figure 4f shows the simulated temperature profiles on the VO_2 and PMMA surface at the SThM bias point, in the center of the device perpendicular to the CNT. The peak temperature in the VO_2 directly underneath the CNT is higher and the temperature rise much more laterally confined than observed on the PMMA surface. Only a few-nanometer wide VO_2 region under the CNT will reach T_{IMT} and trigger the transition, compared to nearly the entire device width when a CNT is not present (Supporting Information Figure S14a). The CNT itself is much hotter, reaching a temperature of ~400 K, but the thermal boundary resistance (between CNT and VO_2) and small contact area limit heat flow from the CNT to the VO_2.

When the series resistance R_S (= 200 kΩ) is added to the model to limit positive feedback, the simulation can also reproduce switching to the metallic state, as shown in Figure 5a for a device with a CNT. These simulations show that the metallic VO_2 forms a narrow conducting "filament," ~10 nm wide, just beneath the CNT. Switching is always triggered beneath the CNT regardless of its location in the VO_2 channel, meaning that using a localized heater can provide a means of control over switching location. Full *I-V* curves for both devices with (Figure 5b) and without (Figure 5c) a CNT can be simulated by sweeping the voltage, where the downwards sweep uses the cooling branch of the *R*(*T*) curve (Figure 1b) to model hysteresis. Both curves reproduce experimental *I-V* behaviour remarkably well, including the differences in switching voltage and hysteresis between the two types of devices, using only Joule heating in the model and no other field effects. Thus combined, our simulations, KPM, SThM, and electrical results suggest that Joule heating is a valid explanation for the mechanism of switching in our devices. Although a thermally-assisted field mechanism cannot be excluded using our data (for example, heating can increase carrier concentration to trigger a Mott transition or reduce the energy barrier for field-induced switching), Joule heating plays a key role in switching devices even in the narrow VO_2 region activated by the hot CNT.

Using this electrothermal model, switching voltage V_{IMT} and current I_{IMT} can be simulated for VO_2 devices without a CNT down to the nanoscale, shown in Figure 5d. The length and width of devices were simultaneously decreased, and a study of the separate effect of length and width may be found in the Supporting Information Section 4b. As the device dimensions are reduced, I_{IMT} steadily decreases and so does V_{IMT} until becoming dominated by contact resistance to the narrow VO_2 stripe. Combined, this results in a linear decrease of switching power P_{IMT} with device size. Adding a CNT to a nanoscale VO_2 device would result in a further reduction in V_{IMT} (especially if the contact resistance to the CNT is low and its heat transfer to the VO_2 is efficient) while slightly increasing I_{IMT}, resulting in a similar overall switching power.

CONCLUSIONS

In summary, we have shown that the IMT switching of VO_2 can be triggered by nanoscale heaters made of individual metallic carbon nanotubes. Two-terminal VO_2 devices with CNTs exhibit switching at less than half the voltage and power of traditional VO_2 devices without a CNT, at all length scales. Using a combination of scanning probe techniques and finite element simulations we studied the origin and scale of the IMT in such devices with and without CNT heaters. Our results are consistent with a Joule heating mechanism in which the CNT locally heats the VO_2 and triggers IMT in narrow region. These results highlight the importance of thermally engineering devices for low-power switching, by using confined heating in small volumes, and are also applicable to a wide variety of thermally-activated phase-change and resistive switching devices.

METHODS

Thin films of single crystalline VO_2 are epitaxially grown on TiO_2 (101) substrates using pulsed laser deposition (PLD), with a nominal thickness of 9 nm.[28] Separately, we grow aligned CNTs with an average diameter of 1.2 nm by chemical vapor deposition (CVD) on ST-cut quartz, then transfer them onto the VO_2.[27] The CNTs on quartz were coated with 100 nm of Au by electron beam (e-beam) evaporation, onto which thermal release tape was pressed (Semiconductor Equipment Corp 1398MS, with adhesion 2.5 N / 20 mm and release temperature 120ºC). The CNT/Au/tape stack was peeled off the quartz and then pressed onto the VO_2. The tape was released on a hot plate at 130ºC, leaving behind the Au-coated CNTs on the VO_2 surface. An O_2 plasma clean (20 sccm, 25 mTorr, 55 W, 3 min) followed by an Ar plasma clean (15 sccm, 12.5 mTorr, 100 W, 3 min) were done to remove tape residue on the Au, with the VO_2 protected from damage by the Au film. The remaining Au was removed using a KI wet etch, leaving behind aligned CNTs on the VO_2. Some carbon-based residue is left after the transfer process (Figure 1e).

The VO_2 and CNTs were patterned into stripes of width W = 3 to 9 μm using a photoresist etch mask. CNTs outside the VO_2 stripes were removed using a light O_2 plasma (20 sccm, 150 mTorr, 30 W, 1 min), then the VO_2 was wet etched for 30 s using a 25% nitric acid solution. Two-terminal devices were fabricated with 50 nm thick Pd contact pads (with no Ti sticking layer) with dimensions 300 μm × 250 μm *via* e-beam evaporation and lift-off, with spacing (device lengths) ranging from L = 3 to 10 μm (Figure 1g). Shorter devices with L = 300 nm to 2 μm were made by adding small extensions of 50 nm thick Pd to the existing pads using e-beam lithography. Presence of metallic CNT(s) in devices was verified electrically and the number of CNTs confirmed by atomic force microscopy (AFM). The VO_2 film thickness after all processing and etching steps is ~5 nm measured by AFM.

Electrical measurements are performed in a micromanipulator probe station from Janis Research under vacuum ($<10^{-4}$ Torr) with a Keithley 4200-SCS parameter analyzer applying a voltage V_S, all at room temperature (T_0 = 296 K) unless otherwise stated. A series resistance R_S = 20 kΩ and 100 kΩ is used for short (< 2 μm long) devices with and without CNTs respectively, and 200 kΩ is used for all other devices. KPM is done on an Asylum Research system with a high voltage module, while the device is biased at a constant voltage. Devices are coated with 50 nm thick 2% 495K PMMA in anisole to carry out passive-mode SThM measurements. PMMA is used rather than an oxide capping layer, because oxide deposition can reduce the stability of the CNT and VO_2. The SThM tip (Pd on SiN, model PR-EX-GLA-5 from Anasys®) is a thermo-resistive element sensitive to electrical discharges, so this capping is necessary in order to electrically isolate the tip from the device while it is biased. SThM is done in passive mode, with a 0.5 V set point and a 0.5 V tip bias.

ASSOCIATED CONTENT

Supporting Information

The Supporting Information is available free of charge on the ACS Publications website at DOI: 10.xxxx/acsnano.xxxxxxx. Additional details of CNT growth and VO2 characterization, additional electrical measurements, discussion of device scaling, discussion of semiconducting and multi-CNT devices, discussion on the use of the series resistor, discussion of contact resistance, additional KPM images, all COMSOL simulation details.

ACKNOWLEDGMENTS

The authors gratefully acknowledge Eilam Yalon and Suhas Kumar for commenting on the manuscript. This work was supported in part by the Stanford SystemX Alliance and by the National Science Foundation (NSF). Work was performed in part at the Stanford Nanofabrication Facility and the Stanford Nano Shared Facilities which receive funding from the NSF as part of the National Nanotechnology Coordinated Infrastructure Award ECCS-1542152. S.B. acknowledges support from the Stanford Graduate Fellowship (SGF) program and the NSERC Postgraduate Scholarship program.

REFERENCES

1. Imada, M.; Fujimori, A.; Tokura, Y., Metal-Insulator Transitions. *Rev. Mod. Phys.* **1998,** *70*, 1039-1263.
2. You, Z.; Ramanathan, S., Mott Memory and Neuromorphic Devices. *Proc. IEEE* **2015,** *103*, 1289-1310.
3. Berglund, C. N.; Guggenheim, H. J., Electronic Properties of VO_2 near the Semiconductor-Metal Transition. *Phys. Rev.* **1969,** *185*, 1022-1033.
4. Kakiuchida, H.; Jin, P.; Nakao, S.; Tazawa, M., Optical Properties of Vanadium Dioxide Film during Semiconductor-Metallic Phase Transition. *Jpn. J. Appl. Phys.* **2007,** *46*, L113-L116.
5. Jerry, M.; Shukla, N.; Paik, H.; Schlom, D. G.; Datta, S., Dynamics of Electrically Driven Sub-Nanosecond Switching in Vanadium Dioxide. *IEEE Silicon Nanoelectron. Workshop*, **2016**.
6. Son, M.; Lee, J.; Park, J.; Shin, J.; Choi, G.; Jung, S.; Lee, W.; Kim, S.; Park, S.; Hwang, H., Excellent Selector Characteristics of Nanoscale VO_2 for High-Density Bipolar ReRAM Applications. *IEEE Electron Device Lett.* **2011,** *32*, 1579-1581.
7. Zhang, K.; Wang, B.; Wang, F.; Han, Y.; Jian, X.; Zhang, H.; Wong, H., VO_2-Based Selection Device for Passive Resistive Random Access Memory Application. *IEEE Electron Device Lett.* **2016,** *37*, 978-981.
8. KuanChang, P.; Weisong, W.; Eunsung, S.; Freeman, K.; Subramanyam, G., Vanadium Oxide Thin-Film Variable Resistor-Based RF Switches. *IEEE Trans. Electron Devices* **2015,** *62*, 2959-2965.
9. Shukla, N.; Thathachary, A. V.; Agrawal, A.; Paik, H.; Aziz, A.; Schlom, D. G.; Gupta, S. K.; Engel-Herbert, R.; Datta, S., A Steep-Slope Transistor Based on Abrupt Electronic Phase Transition. *Nat. Commun.* **2015,** *6*, 7812.
10. Vitale, W. A.; Casu, E. A.; Biswas, A.; Rosca, T.; Alper, C.; Krammer, A.; Luong, G. V.; Zhao, Q. T.; Mantl, S.; Schuler, A.; Ionescu, A. M., A Steep-Slope Transistor Combining Phase-Change and Band-to-Band-Tunneling to Achieve a Sub-Unity Body Factor. *Sci. Rep.* **2017,** *7*, 355.
11. Shukla, N.; Parihar, A.; Freeman, E.; Paik, H.; Stone, G.; Narayanan, V.; Wen, H.; Cai, Z.; Gopalan, V.; Engel-Herbert, R.; Schlom, D. G.; Raychowdhury, A.; Datta, S., Synchronized Charge Oscillations in Correlated Electron Systems. *Sci. Rep.* **2014,** *4*, 4964.
12. Yi, W.; Tsang, K. K.; Lam, S. K.; Bai, X.; Crowell, J. A.; Flores, E. A., Biological Plausibility and Stochasticity in Scalable VO_2 Active Memristor Neurons. *Nat. Commun.* **2018,** *9*, 4661.
13. Liu, L.; Kang, L.; Mayer, T. S.; Werner, D. H., Hybrid Metamaterials for Electrically Triggered Multifunctional Control. *Nat. Commun.* **2016,** *7*, 13236.
14. Kats, M. A.; Blanchard, R.; Genevet, P.; Yang, Z.; Qazilbash, M. M.; Basov, D. N.; Ramanathan, S.; Capasso, F., Thermal Tuning of Mid-Infrared Plasmonic Antenna Arrays Using a Phase Change Material. *Opt. Express* **2013,** *38*, 368-370.
15. Seo, M.; Kyoung, J.; Park, H.; Koo, S.; Kim, H. S.; Bernien, H.; Kim, B. J.; Choe, J. H.; Ahn, Y. H.; Kim, H. T.; Park, N.; Park, Q. H.; Ahn, K.; Kim, D. S., Active Terahertz Nanoantennas Based on VO_2 Phase Transition. *Nano Lett.* **2010,** *10*, 2064-2068.
16. Kats, M. A.; Blanchard, R.; Zhang, S.; Genevet, P.; Ko, C.; Ramanathan, S.; Capasso, F., Vanadium Dioxide as a Natural Disordered Metamaterial: Perfect Thermal Emission and Large Broadband Negative Differential Thermal Emittance. *Phys. Rev. X* **2013,** *3*, 041004.
17. Joushaghani, A.; Jeong, J.; Paradis, S.; Alain, D.; Stewart Aitchison, J.; Poon, J. K. S., Voltage-Controlled Switching and Thermal Effects in VO_2 Nano-Gap Junctions. *Appl. Phys. Lett.* **2014,** *104*, 221904.
18. Radu, I. P.; Govoreanu, B.; Mertens, S.; Shi, X.; Cantoro, M.; Schaekers, M.; Jurczak, M.; De Gendt, S.; Stesmans, A.; Kittl, J. A.; Heyns, M.; Martens, K., Switching Mechanism in Two-Terminal Vanadium Dioxide Devices. *Nanotechnology* **2015,** *26*, 165202.
19. Aetukuri, N. P. B. The Control of Metal-Insulator Transition in Vanadium Dioxide. Ph.D. Thesis, Stanford University, 2013.

20. Raoux, S.; Xiong, F.; Wuttig, M.; Pop, E., Phase Change Materials and Phase Change Memory. *MRS Bull.* **2014,** *39*, 703-710.
21. Xiong, F.; Liao, A. D.; Estrada, D.; Pop, E., Low-Power Switching of Phase-Change Materials with Carbon Nanotube Electrodes. *Science* **2011,** *332*, 568-570.
22. Li, D.; Sharma, A. A.; Gala, D. K.; Shukla, N.; Paik, H.; Datta, S.; Schlom, D. G.; Bain, J. A.; Skowronski, M., Joule Heating-Induced Metal-Insulator Transition in Epitaxial VO_2/TiO_2 Devices. *ACS Appl. Mater. Interfaces* **2016,** *8*, 12908-12914.
23. Stefanovich, G.; Pergament, A.; Stefanovich, D., Electrical Switching and Mott Transition in VO_2. *J. Phys.: Condens. Matter* **2000,** *12*, 8837-8845.
24. Chen, F. H.; Fan, L. L.; Chen, S.; Liao, G. M.; Chen, Y. L.; Wu, P.; Song, L.; Zou, C. W.; Wu, Z. Y., Control of the Metal-Insulator Transition in VO_2 Epitaxial Film by Modifying Carrier Density. *ACS Appl. Mater. Interfaces* **2015,** *7*, 6875-6881.
25. Liao, A.; Alizadegan, R.; Ong, Z.-Y.; Dutta, S.; Xiong, F.; Hsia, K. J.; Pop, E., Thermal Dissipation and Variability in Electrical Breakdown of Carbon Nanotube Devices. *Phys. Rev. B* **2010,** *82*, 205406.
26. Xiong, F.; Liao, A.; Pop, E., Inducing Chalcogenide Phase Change with Ultra-Narrow Carbon Nanotube Heaters. *Appl. Phys. Lett.* **2009,** *95*, 243103.
27. Patil, N.; Lin, A.; Myers, E. R.; Koungmin, R.; Badmaev, A.; Chongwu, Z.; Wong, H. S. P.; Mitra, S., Wafer-Scale Growth and Transfer of Aligned Single-Walled Carbon Nanotubes. *IEEE Trans. Nanotechnol.* **2009,** *8*, 498-504.
28. Jeong, J.; Aetukuri, N.; Graf, T.; Schladt, T. D.; Samant, M. G.; Parkin, S. S., Suppression of Metal-Insulator Transition in VO_2 by Electric Field-Induced Oxygen Vacancy Formation. *Science* **2013,** *339*, 1402-1405.
29. Pop, E.; Mann, D. A.; Goodson, K. E.; Dai, H., Electrical and Thermal Transport in Metallic Single-Wall Carbon Nanotubes on Insulating Substrates. *J. Appl. Phys.* **2007,** *101*, 093710.
30. Martens, K.; Radu, I. P.; Mertens, S.; Shi, X.; Nyns, L.; Cosemans, S.; Favia, P.; Bender, H.; Conard, T.; Schaekers, M.; De Gendt, S.; Afanas'ev, V.; Kittl, J. A.; Heyns, M.; Jurczak, M., The VO_2 Interface, the Metal-Insulator Transition Tunnel Junction, and the Metal-Insulator Transition Switch On-Off Resistance. *J. Appl. Phys.* **2012,** *112*, 124501.
31. Percy, R.; Kittiwatanakul, S.; Lu, J.; Stan, M.; Wolf, S.; Weikle, R. M., Method for Characterizing the Contact Resistance of Metal-Vanadium Dioxide Thin Film Interfaces. *Appl. Phys. Lett.* **2014,** *105*, 021603.
32. Jeong, J.; Yong, Z.; Joushaghani, A.; Tsukernik, A.; Paradis, S.; Alain, D.; Poon, J. K., Current Induced Polycrystalline-to-Crystalline Transformation in Vanadium Dioxide Nanowires. *Sci. Rep.* **2016,** *6*, 37296.
33. Sadewasser, S.; Glatzel, T., *Kelvin Probe Force Microscopy: Measuring and Compensating Electrostatic Forces*; Springer: Heidelberg, 2011.
34. Borca-Tasciuc, T., Scanning Probe Methods for Thermal and Thermoelectric Property Measurements. *Annu. Rev. Heat Transfer* **2013,** *16*, 211-258.
35. Yalon, E.; Deshmukh, S.; Munoz Rojo, M.; Lian, F.; Neumann, C. M.; Xiong, F.; Pop, E., Spatially Resolved Thermometry of Resistive Memory Devices. *Sci. Rep.* **2017,** *7*, 15360.

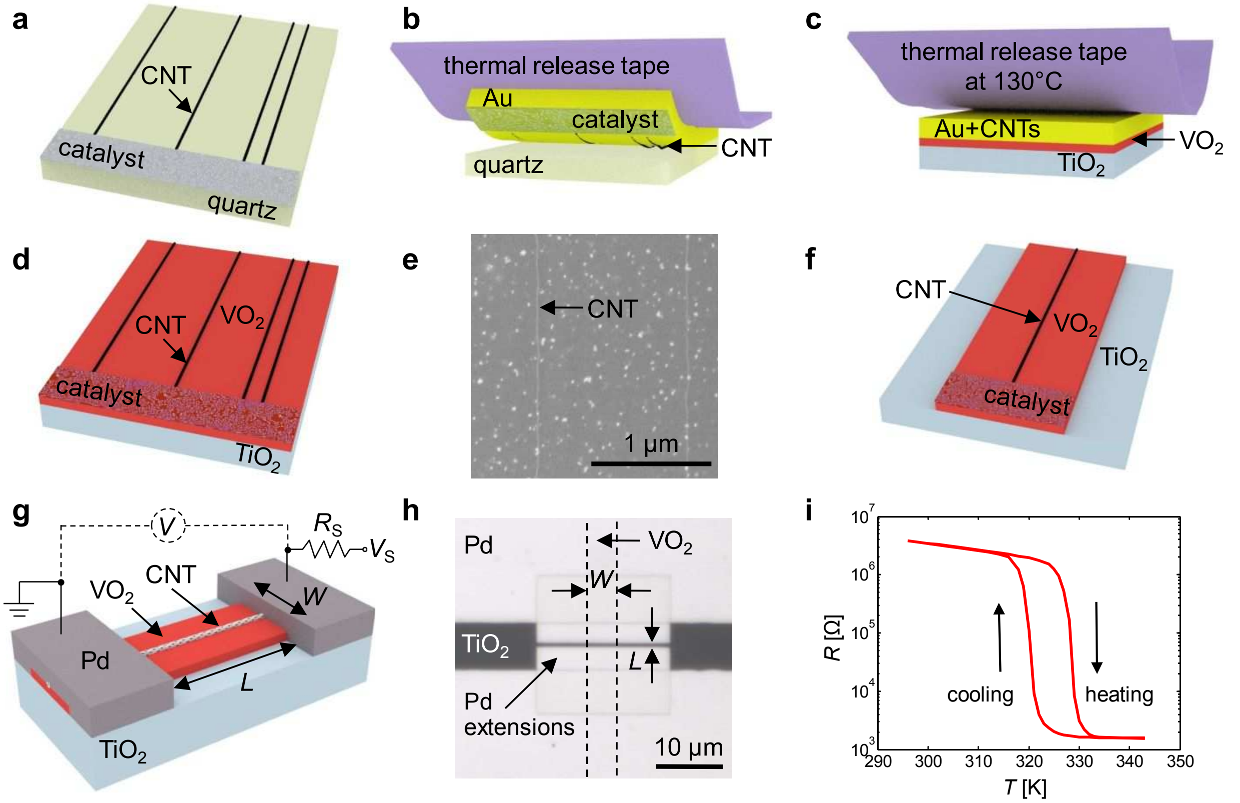

Figure 1. Fabrication Process (layers are not to scale). (a) Aligned carbon nanotubes (CNTs) are grown on ST-cut quartz *via* CVD, with Fe catalyst particles.[27] (b) Au is e-beam evaporated onto the CNTs, then peeled off the quartz using thermal release tape. (c) The Au-coated CNTs are pressed onto VO_2 grown epitaxially by PLD on TiO_2.[28] The thermal release tape is then removed by heating to 130°C. (d) After a plasma clean to remove tape residue, the Au is wet-etched, leaving behind CNTs on VO_2. (e) Scanning electron microscope (SEM) image of CNTs on VO_2. The small dots are residue left by the transfer process. (f) Excess CNTs outside planned VO_2 stripes are removed with an O_2 plasma then the VO_2 is wet etched in diluted nitric acid. (g) Schematic of a fabricated VO_2 device with CNT heater and measurement setup, after e-beam evaporation and lift-off of Pd contacts. The width, *W*, and length, *L*, of the patterned VO2 region are as labeled. The thickness of the VO_2 is ~5 nm in finished devices after all processing steps. Similar control devices were fabricated without CNT heaters. (h) For shorter devices, additional Pd contact extensions are added. Optical image of a short (L = 520 nm, W = 3.9 μm) VO_2 device. (i) Measured resistance of a VO_2 device without a CNT heater as a function of stage temperature. (L = 5 μm, W = 7 μm)

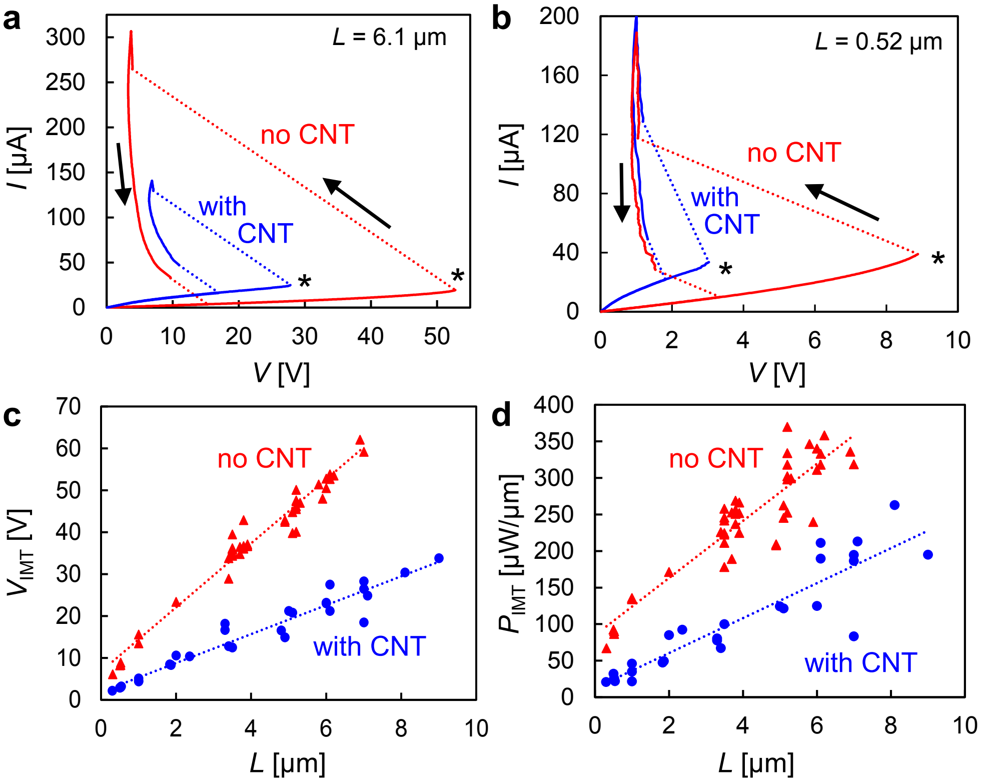

Figure 2. Electrical switching of devices with and without a CNT. (a) Typical switching of "long" devices with and without a CNT (*L* = 6.1 μm, *W* = 3.2 μm) using DC voltage control. (b) Typical switching of "short" devices with and without a CNT (*L* = 520 nm, *W* = 4 μm) using DC voltage control. The short devices and the devices with a CNT heater have much lower switching voltages, V_{IMT}, labeled with * on the figures. Arrows show voltage sweep directions, and dashed lines indicate snapbacks. (c) Measured V_{IMT} as a function of length for devices with (blue circles) and without (red triangles) a CNT. Dotted lines represent a linear fit. (d) Switching power, P_{IMT}, normalized by VO_2 width, for devices with (blue circles) and without (red triangles) a CNT. The dotted lines represent a linear fit. Adding a CNT approximately halves switching power at all length scales.

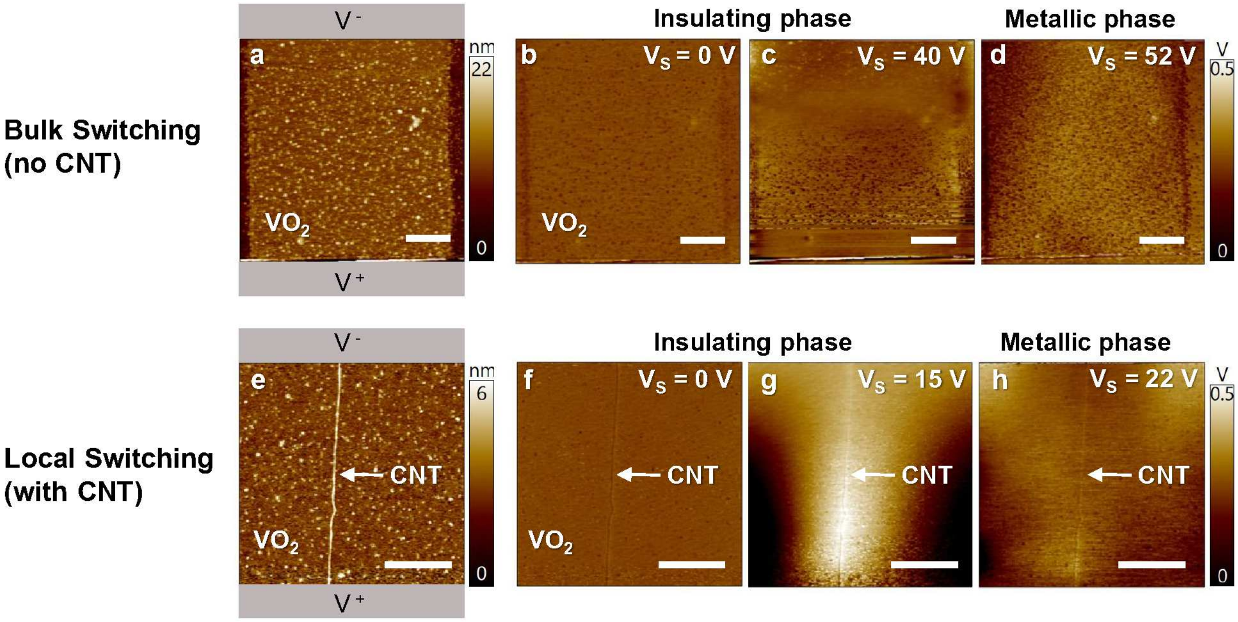

Figure 3. Topography and Kelvin Probe Microscopy (KPM) of VO_2 devices with and without CNT. (a) Topography of VO_2 control device without a CNT. (b – d) Flattened KPM images of the same device with increasing bias. The Pd electrodes are outside the top and bottom margin of the device images, biased as marked. (e) Topography of VO_2 device with a single metallic CNT, indicated by the arrow. (f – h) Flattened KPM images of the same device with increasing bias, revealing localized switching caused by the CNT. All scale bars are 1 μm.

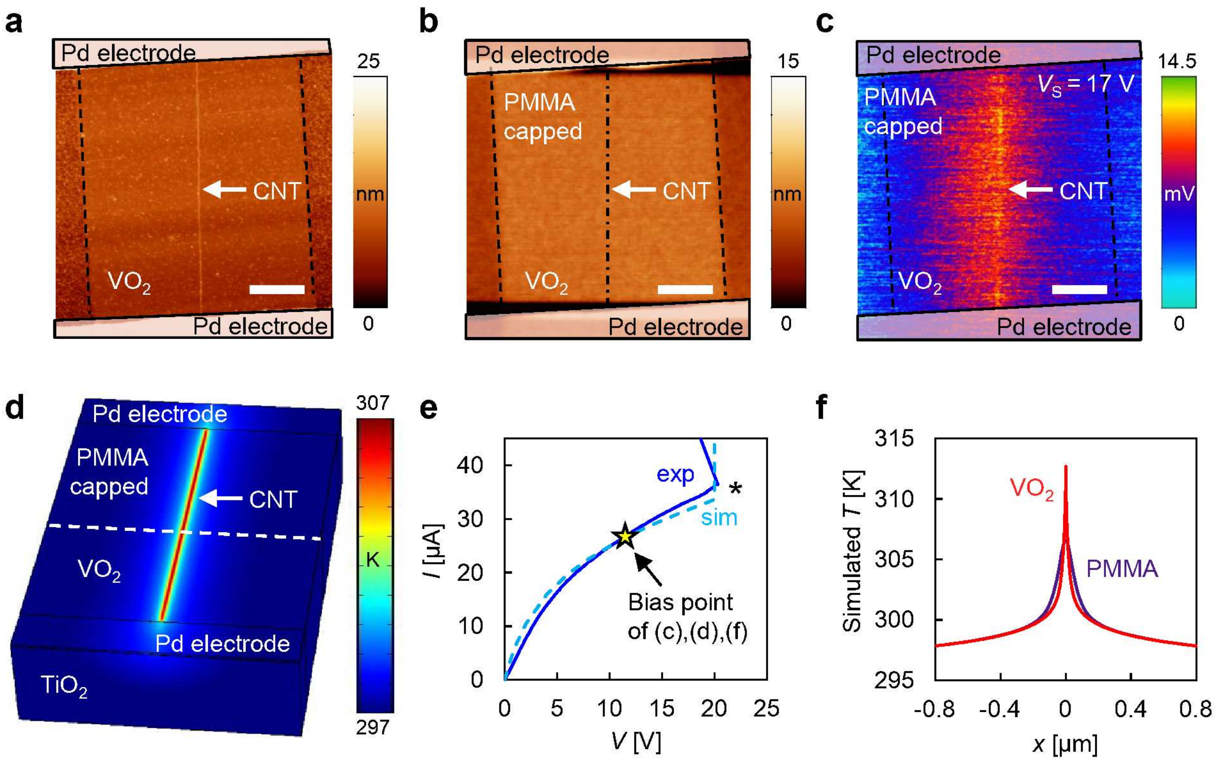

Figure 4. (a) Topography of an unbiased device with a single metallic CNT. (b) Topography of the same device covered in 50 nm of PMMA, with the CNT no longer visible. (c) Scanning thermal microscopy of the device under bias, prior to the metallic transition which occurs at V_S = 27 V (V_{IMT} = 20.3 V). (d) Simulated surface temperature of the device on top of the PMMA, at the same bias voltage. (e) *I*-*V* characteristics of the device (solid blue) compared to the model (dashed light blue), with switching marked by a *. (f) Simulated temperature profile across the VO$_2$ (red) and on the PMMA surface (purple) perpendicular to the CNT along the dashed white line in (d). Scale bars are 1.5 μm.

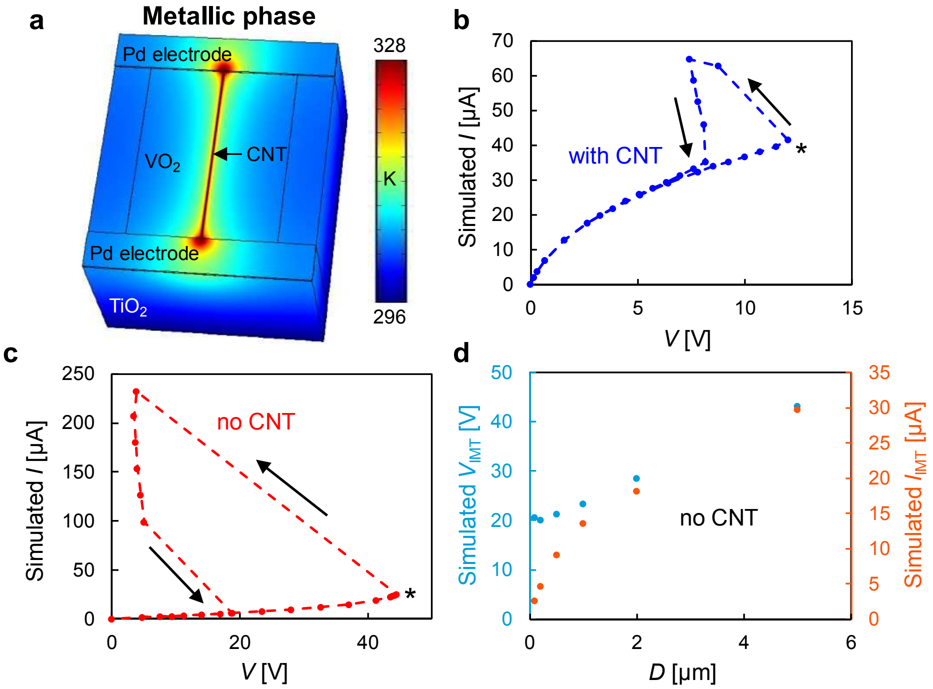

Figure 5. (a) Simulated temperature on the surface of a device with a CNT (L = 5 μm, W = 4 μm) after the metallic transition, with Rs = 200 kΩ. (b) Simulated I-V curve of a device with a CNT using voltage control, including hysteresis. (c) Simulated I-V curve of a device without a CNT using voltage control, including hysteresis. The switching voltage (*) is much higher without the CNT to act as a heater. (d) Simulated switching voltage V_{IMT} and current I_{IMT} for devices without a CNT as the device dimensions D are reduced (L=W are simultaneously reduced).

Table of Contents (TOC) Figure: